Structure, Vol. 11, 1609–1620, December, 2003, ©2003 Elsevier Science Ltd. All rights reserved. DOI 10.1016/j.str.2003.10.014

The First Structure of an RNA m^{5}C Methyltransferase, Fmu, Provides Insight into Catalytic Mechanism and Specific Binding of RNA Substrate

Paul G. Foster,[1,3,4] Christa R. Nunes,[2,3] Patricia Greene,[1] Demetri Moustakas,[2] and Robert M. Stroud[1,*]
[1]Department of Biochemistry and Biophysics
[2]Bioengineering Graduate Group
University of California, San Francisco
San Francisco, California 94148

Summary

The crystal structure of *E. coli* Fmu, determined at 1.65 Å resolution for the apoenzyme and 2.1 Å resolution in complex with AdoMet, is the first representative of the 5-methylcytosine RNA methyltransferase family that includes the human nucleolar proliferation-associated protein p120. Fmu contains three subdomains which share structural homology to DNA m$_5$C methyltransferases and two RNA binding protein families. In the binary complex, the AdoMet cofactor is positioned within the active site near a novel arrangement of two conserved cysteines that function in cytosine methylation. The site is surrounded by a positively charged cleft large enough to bind its unique target stem loop within 16S rRNA. Docking of this stem loop RNA into the structure followed by molecular mechanics shows that the Fmu structure is consistent with binding to the folded RNA substrate.

Introduction

A variety of RNA-modifying enzymes function in the posttranslational maturation of ribosomal RNA, with the most common modifications resulting in the site-specific methylation of nucleosides. Of the 37 known modifications present in *Escherichia coli* ribosomal RNA, 4 are 2′-O-methylnucleosides and 21 are selected base methylations (Rozenski et al., 1999). Three of the twenty-one methylated bases in rRNA are 5-methylcytosine (m^{5}C). These sites include m^{5}C967 of 16S RNA of the small ribosomal subunit. m^{5}C967 is found in a conserved 8 base loop that is implicated in tRNA binding within the P site of the mRNA-tRNA-ribosome complex (Yusupov et al., 2001). The methylation at 967 is catalyzed by the *E. coli* protein Fmu (Gu et al., 1999; Tscherne et al., 1999).

Fmu is a member of a superfamily of S-adenosyl-L-methionine (AdoMet)-dependent methyltransferases (MTases) that act on a variety of small molecule, protein, and nucleic acid substrates. Structural data show that the core catalytic domain of these MTases is composed of a common structure reminiscent of the Rossmann fold. Sequence alignments of the catalytic domains of known RNA and DNA MTases exhibit up to ten sequence motifs, designated I–X, for which functions have been assigned from structural studies (reviewed in Fauman et al., 1999). Motifs I–V are involved in AdoMet binding; motifs IV, VI, and VIII contain signature sequences that target specific bases. A search of sequence databases revealed a large family of Fmu homologs, which are putative m^{5}C RNA MTases (Reid et al., 1999). Sequence alignment of the Fmu homologs shows a common core region that contains the AdoMet binding domain plus a conserved motif designated "N1." This family also contains variable N-terminal and/or C-terminal extensions that allow separation into eight subfamilies. Fmu is a member of a widespread Eubacterial subfamily of enzymes that presumably modify the same base in 16S RNA. Nop2p of *S. cerevesiae* and the human nucleolar proliferation-associated protein p120 are members of a second subfamily, and both appear to be necessary for assembly of 23S RNA into the large ribosomal subunit (Gustafson et al., 1998; Hong et al., 1997). Of particular interest is the finding that p120 is overexpressed in most tumor cells, and its inhibition has demonstrated a decrease in cell growth (Perlaky et al., 1996; Sato et al., 1999), suggesting it might serve as a novel target for therapeutic intervention.

Enzymes that methylate the C5 position of pyrimidines utilize the thiolate of cysteine to attack the 6-carbon of the target pyrimidine base, forming a Michael adduct and thereby activating the 5-carbon for methyl transfer (Ivanetich and Santi, 1992). All m^{5}C DNA MTases contain the catalytic cysteine within an absolutely conserved ProCys dipeptide in motif IV (Cheng, 1995). A homologous ProCys dipeptide is found in motif IV of Fmu (residues 324–325), and it is conserved in all but one of the other RNA m^{5}C MTase subfamilies, where it becomes ProSerCys. Yet all RNA m^{5}C MTases also contain a second absolutely conserved cysteine (Cys 375) within a ThrCys dipeptide in motif VI. Cys 375 within the RNA m^{5}C MTases is in the same position as the catalytic cysteine of another AdoMet-dependent enzyme, tRNA m^{5}U54 MTase (RUMT) (Kealey and Santi, 1991), and this motif VI cysteine has also been shown to be the catalytic nucleophile in Fmu (Liu and Santi, 2000). Since these two divergent RNA MTases utilize the same cysteine nucleophile, Liu and Santi surmised that the motif VI cysteine would be the "universal" nucleophile of all of the RNA m^{5}U and RNA m^{5}C MTases.

We determined the crystal structures of *E. coli* Fmu in the unliganded and AdoMet-bound forms, the first three-dimensional structure of any RNA m^{5}C MTase. Fmu consists of three domains, including an N-terminal domain related to the NusB RNA binding protein, a small central domain, and a C-terminal MTase domain. The structure reveals an active site in which the two conserved cysteine residues are both accessible and closely positioned near the activated methyl of the cofactor. While one of these cysteine residues functions as the catalytic nucleophile, the spatial arrangement suggests that the second cysteine residue also plays an active role in the methyltransferase mechanism.

*Correspondence: stroud@msg.ucsf.edu
[3]These authors contributed equally to this work.
[4]Present address: Exelixis, Inc., 170 Harbor Way Box 0511, South San Francisco, California 94083.

Table 1. Crystallographic Statistics

Data Collection Statistics[a]

Dataset	Native	SeMet, λ_1	SeMet, λ_2	SeMet, λ_3	AdoMet
Wavelength	0.92100	0.97962	0.97976	0.96112	0.92100
Resolution (Å)	1.65 (1.68–1.65)	2.25 (2.29–2.25)	2.4 (2.44–2.40)	2.4 (2.44–2.40)	2.0 (2.03–2.00)
Observations	301,824	73,114	61,059	48,337	202,474
Unique	56,794	38,756	38,802	26,107	31,507
Completeness (%)	98.6 (79.6)	87.6 (76.5)	88.6 (84.3)	71.5 (67.0)	
R_{sym} (%)[b]	4.5 (29.0)	9.5 (35.1)	8.2 (43.8)	9.2 (56.9)	4.3 (32.7)
Average I/σI	23.6 (3.5)	14.2 (2.7)	15.8 (3.9)	13.6 (2.0)	18.9 (1.6)
Mad Analysis					
MAD phasing resolution (Å)		20–2.4			
Number of Se sites		14			

Overall Isomorphous and Dispersive Differences — Phasing Power[c]

Wavelength	SeMet, λ_1	SeMet, λ_2	SeMet, λ_3	Iso	Ano
SeMet, λ_1	0.1197	0.1028	0.1443	0.00	1.79
SeMet, λ_2		0.0772	0.0928	0.80	1.68
SeMet, λ_3			0.0623	1.98	1.26
R_{cullis}[d]		0.74			
Overall figure of merit to 2.4		0.56			

Refinement Statistics

Dataset	Native	AdoMet
No. of reflections, F > σF (working/test)	53,354/2,799	28,489/2,555
No. of nonhydrogen atoms	3,678	3,416
Resolution (Å)	30.0–1.65	30–2.00
R_{cryst}/R_{free}[e](%)	21.8/25.6	23.1/27.6
Rms deviation for bond lengths (Å)	0.009	0.021
Rms deviation for bond angles (°)	1.316	2.002

[a] Values in parentheses refer to data in the highest resolution bin.
[b] $R_{sym} = \Sigma(|(I - <I>)|)/\Sigma(I)$.
[c] Phasing power (iso/ano) = $(\Sigma|F_H|/\Sigma|\epsilon|)/(\Sigma\{2|F_H^{II}|\}/\Sigma|\epsilon|)$.
[d] $R_{cullis} = \Sigma((|F_{PH}|(obs) \pm |F_P|(obs)) - |F_H|(calc))/(|F_{PH}|(obs) \pm |F_P|(obs))$.
[e] $R_{cryst} = \Sigma(|(I - <I>)|)/\Sigma(I)$. R_{free} was calculated for a subset of reflections (5%) omitted from the refinement.

Results and Discussion

Overall Structure of the *E. coli* Apo-Fmu and *E. coli* Fmu-AdoMet Complex

An initial model for the Fmu apoenzyme was determined using multiwavelength anomalous dispersion (MAD) phasing and 2-fold NCS averaging from selenomethionine-labeled crystals which diffracted to 2.25 Å resolution (Table 1). The partial MAD model, which corresponded to ca. 80% of the Fmu molecule, was then used as a search model for molecular replacement against a native data set extending to 1.65 Å resolution. The resulting 1.65 Å Fmu structure refined to a final R factor of 21.8% (R_{free} = 25.6%) and comprises residues Arg 5-Lys 428 and 390 water molecules. No attempts were made to remove AdoMet during protein purification, but neither the SeMet Fmu structure nor the final 1.65 Å structure, revealed any density for the cofactor in the active site. Therefore, crystals were grown in the presence of the cofactor, and the structure of AdoMet-bound Fmu was determined to 2.1 Å resolution by molecular replacement and difference fourier analysis. The Fmu-AdoMet structure was refined to an R factor of 23.7% (R_{free} = 27.5%), with observed density for residues Arg 5-Lys 429 and 115 water molecules. Alignment of the apo Fmu structure and Fmu-AdoMet complex indicated that the two structures were nearly identical, with an overall root-mean-square (rms) deviation of ~0.7 Å between all corresponding C_α positions, with the largest deviations (>1 Å) occurring at the AdoMet binding site.

The Fmu monomer consists of three domains that form a bilobed molecule with dimensions of 71 × 48 × 30 Å (Figure 1). The smaller lobe of the molecule is formed by an all α-helical N-terminal domain (residues 5–145) that differentiates the Fmu subfamily from other RNA m^5C MTases. The larger lobe of Fmu consists of the core region observed in all RNA m^5C MTases, and it is composed of a small domain (residues 173–231) that contains the conserved sequence motif designated "N1" (Reid et al., 1999), plus the larger, catalytic C-terminal domain (residues 232–429). The two lobes of the enzyme are connected via two short helices (residues 146–172) that contain several hydrophobic residues conserved in the Fmu subfamily that includes Trp 148, Leu 149, Val 150, Tyr 157, and Ile 164. The three-dimensional arrangement of the three domains generates a large groove along the surface of the protein. The AdoMet cofactor is located in a pocket found along the side of the groove formed by the MTase domain, with its activated methyl group positioned near both Cys 325 and the catalytic Cys 375. Analysis of the electrostatic potential indicates a positive surface around the active site groove and N-terminal domain, and the dimensions of the groove (~25 Å long × 15 Å wide × 10 Å deep)

suggest it is capable of binding the folded RNA substrate, assuming that the target cytosine base is positioned near the cofactor.

An N-Terminal RNA Binding Domain

The Fmu subfamily is distinguished from other putative RNA m^{5}C MTase subfamilies by an N-terminal sequence extension. The structure of this domain is comprised of eight α helices packed into a globular bundle with dimensions of 41 $\times$ 41 $\times$ 45 Å, with a hydrophobic core maintained by several conserved residues, principally Tyr 86, Tyr 90, Val 102, Val 121, and Leu 122 (Figure 2A). The three-dimensional arrangement of the helices demonstrates a structural repeat of two 65 residue segments, with each repeat corresponding to four α helices aligned over 56 equivalent C_α atoms with an rms deviation of 1.836 Å (Kleywegt and Jones, 1997) (Figure 2A). There is no sequence homology apparent for the two structurally aligned segments, and thus there is no evidence that the structural repeat is the result of a gene duplication event.

The N-terminal sequence of Fmu shares homology to another (noncatalytic) RNA binding protein, the ribosomal RNA antiterminator protein NusB (Gopal et al., 2000). Alignment of the Fmu N-terminal domain with the structure of NusB from *Mycobacterium tuberculosis* demonstrates that the two domains share the same fold (Figure 2B), with an rmsd of 1.54 Å for 95 C_α atoms that extends over six of seven helices common to both proteins. Despite the structural homology between the two domains, the intradomain repeat observed in Fmu is less obvious in the NusB monomer, where only four of the seven helices of NusB can be internally aligned (helix A with helix E and helix C with helix G). Helix B of NusB does not align with the helix F, but this is likely due to the fact that helix B is involved in NusB dimerization. Although the overall sequence conservation between Fmu and NusB is weak (25% identity), all sequences in the Fmu subfamily demonstrate a preponderance of basic residues at the N terminus of this domain, similar to the arginine-rich phosphate binding site present at the N terminus of NusB (Gopal et al., 2000). The combination of structural similarity and conservation of basic residues between the two domains supports an RNA binding role for the N terminus of Fmu.

The Central "N1" Domain

The catalytic lobe of Fmu comprises the conserved core identified in all of the putative RNA m^{5}C MTase sequences. It begins with a small domain ($\sim$60 amino acids) that contains the conserved "N1" sequence motif followed by a MTase domain. The "N1" domain adopts a $\beta\alpha\beta\beta\alpha\beta$ topology reminiscent of the RNA recognition motif (RRM) observed in a large number of RNA binding proteins, with two helices packed to one side of an antiparallel β sheet with right-hand twist. A comparison with a nonredundant database of known structures (DALI 2.0) (Holm and Sander, 1993) indicates weak structural homology to other RNA binding domains (Z score $<$ 4) such as the U1A splicesomal protein and hnRNP A1 protein.

Although the N1 domain is structurally homologous to known RNA binding proteins, there is no clear sequence motif that defines its role in RNA binding and recognition. Only one completely conserved residue, Arg 177, is accessible to solvent. It is positioned within 8 Å from the carboxyl moiety of AdoMet, which suggests a possible role in binding the phosphate backbone of the RNA. The N1 domain makes extensive contact with the catalytic MTase domain, an interaction that buries a combined surface area of $\sim$560 A^2. This corresponds to approximately half of the total surface area of the N1 domain, and demonstrates that the two domains form a common structural core. In contrast, the N-terminal domain makes little direct contact with the MTase domain (total buried surface area of 250 A^2) and no contact with the N1 domain. In spite of the lack of a conserved RNA binding motif, the close association of the N1 and MTase domains suggest that any RNA bound in the active site of the MTase domain is likely to interact with the N1 domain.

The Fmu MTase Domain

At the functional center of the catalytic lobe is the MTase domain of Fmu (residues 232–429), which adopts a fold typical of known AdoMet-dependent methyltransferases. The topology is a mixed seven-stranded β sheet arranged in the order 7-6-5-8-9-11-10, with all stands parallel except β11. Within the β sheet, this order corresponds to the most common 3-2-1-4-5-7-6 arrangement of strands observed in the "universal" MTase core (Fauman et al., 1999). The β sheet is sandwiched on each side by three α helices: helices M, N, and O pack against the side of the sheet that faces the central cleft, while helices P, R, and S are positioned along the surface of the molecule (Figure 3A). The M, N, and O helices also pack against the β sheet of the N1 domain.

The Fmu MTase domain demonstrates highest structural similarity to other RNA MTases, including two putative 2′-O RNA MTases, fibrillarin-homolog from *M. jannaschi* (Wang et al., 2000a), and *E.coli* ftsJ (Bügl et al., 2000) (Z scores of 15.8 and 13.5, respectively). However, the catalytic and substrate binding features of Fmu that target m^{5}C formation are more similar in structure to the corresponding regions of the DNA m^{5}C MTases. For example, both Fmu and the DNA m^{5}C MTases have an extended loop (18–19 residues) that connects strand β8 to αR. In the 2′-O RNA MTases and the RNA m^{N6}A MTases, no catalytic residue is needed to activate the substrates for methylation, and the corresponding loop observed in these structures is only 3–9 residues in length (Bussiere et al., 1998; Schluckebier et al., 1997; Wang et al., 2000a). In the DNA m^{5}C MTases, this loop contains the catalytic cysteine (motif IV), and it undergoes a large conformational shift upon binding its DNA substrate that brings the cysteine residue into contact with the target cytosine base (Cheng et al., 1993a, 1993b; Klimasauskas et al., 1994). It is noteworthy, however, that in Fmu this loop contains not only the conserved Cys 325 of motif IV but also helix Q, which provides the only direct packing interactions between the helical N-terminal domain and the catalytic lobe and is conserved in the Fmu RNA m^{5}C MTase family. Thus, the interaction of helix Q with the N-terminal domain

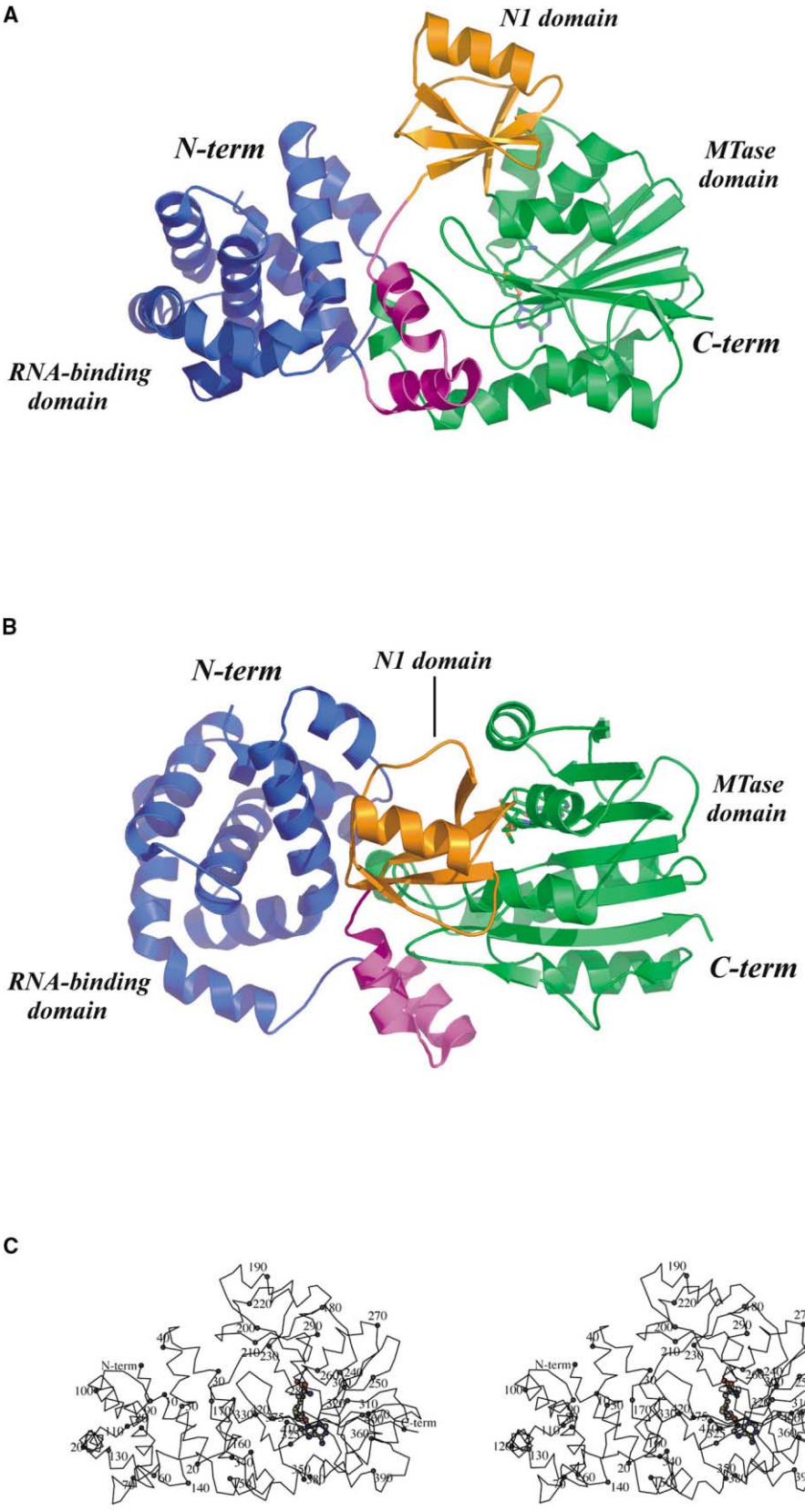

Figure 1. The Overall Structure of Fmu Presents a Bilobed Molecule with a Large Central Cleft

(A) Ribbon diagram of the Fmu monomer with the cofactor AdoMet in ball-and-stick representation. The molecule consists of three distinct domains, though the N1 domain (orange) has extensive contacts with the C-terminal MTase domain (green). The α-helical N-terminal domain

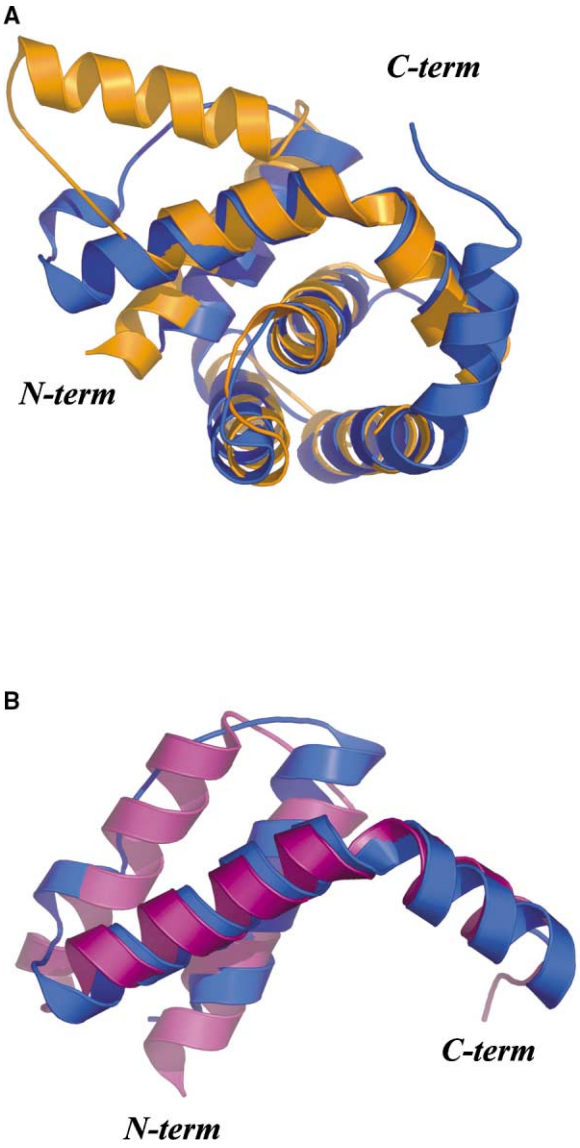

Figure 2. The N-Terminal Region of Fmu Is an RNA Binding Domain Built from a Structural Repeat

(A) Superposition of the Fmu N-terminal domain (blue) with the crystal structure of the rRNA antiterminator protein NusB from *Mycobacterium tuberculosis* (orange). Structural alignment demonstrates a clear similarity in the protein folds with an overall rmsd of 1.54 Å for 95 C_α positions.

(B) The structural repeat within the N-terminal domain of Fmu as demonstrated by a superposition of residues 5–70 (blue) and 75–145 (magenta). The alignment of the two halves of the domain gives an overall rmsd of 1.84 Å for 56 C_α positions, although no sequence similarity can be observed between the two regions.

positions the motif IV loop of Fmu in a conformation similar to motif IV of the DNA m5C MTase ternary complex, suggesting that the motif IV loop does not undergo a major conformational change upon binding substrate and that the active site of Fmu is properly ordered to bind the RNA substrate.

A Conserved Binding Pocket for AdoMet

As in other MTase structures, AdoMet binds in a pocket at the C-terminal ends of strands β5–β7 where the conserved residues of motifs I–III are located (Figure 3B). Motif I, which adopts a tight hairpin turn that connects β5 and αN, functions to coordinate the carboxylate of AdoMet via the backbone nitrogens of Pro 257, Gly 258, and Gly 259, and a side chain amine of Lys 260 (Figure 4A). In addition, motif I contains the conserved residues Leu 253 and Cys 254, which form part of the hydrophobic pocket that binds the adenine ring. Motif II, located at the end of β6, coordinates the ribose hydroxyls through the carboxylate side chain of Asp 277 and the guanidinium of Arg 282. It also provides Van der Waals interactions with the adenine base through the side chain of Ile 278. Motif III, found at the C terminus of strand β7, coordinates the N6 and N1 of the adenine base through the side chain of Asp 303 and the backbone NH of Gly 304, respectively.

In addition to the specific AdoMet binding residues of motifs I–III, two other motifs present in Fmu and various DNA/RNA MTases provide residues that compose the remainder of the AdoMet binding pocket. Motif IV, located at the end of β8, contains Asp 322, which hydrogen bonds to the amino end of the AdoMet, while Leu 321 and Pro 324 pack against the adenine base. Motif V is represented by two conserved residues found within αR, Leu 352, and Ile 356. These residues present a hydrophobic surface along one edge of the AdoMet binding site and are in contact with the adenine.

The position and orientation of the AdoMet cofactor within the Fmu structure is similar to that observed in the DNA m5C MTase HhaI ternary complex with DNA (Klimasauskas et al., 1994), except the adenine base is rotated slightly and shifted by 1 Å within the binding pocket (Figure 4B). The shift in the cofactor position is primarily due to a change in packing interactions on the face of the adenine ring, in which the conserved Phe18 of motif I in the DNA m5C MTase family is replaced by the smaller Cys 254 in the RNA m5C MTases. Despite the shift of the adenine base, the position of the methyl group in both structures is nearly identical suggesting that the AdoMet in the Fmu-AdoMet binary complex is in a position that could be competent for methyl transfer. Thus, the Fmu binary complex contrasts with the HhaI DNA MTase binary complex where AdoMet is bound in a nonproductive orientation (Cheng et al., 1993b).

(blue) presents a sizeable surface area to bind the folded rRNA substrate. Its main connection to the C-terminal lobe is through two short helices (magenta) at the base of the molecule.

(B) Top view of Fmu, similar to that of Figure 1A, except rotated about the *x* axis by 90°.

(C) Stereo C_α trace of the Fmu-AdoMet complex with landmark residues identified by amino acid sequence numbers. The orientation is similar to that of Figure 1A rotated −90° around the *z* axis. All ribbon diagrams were generated with the graphics program PyMOL (Delano Scientific).

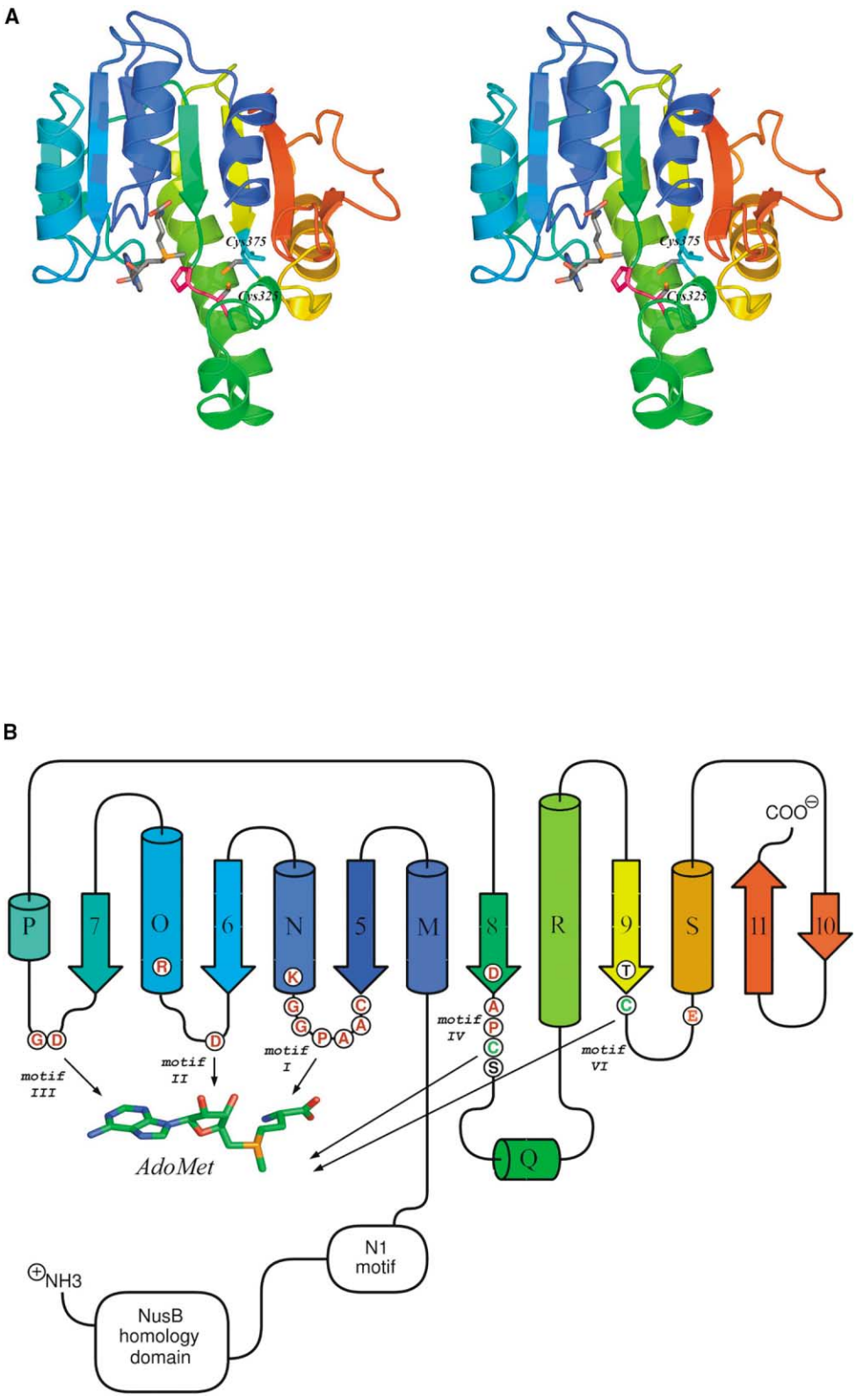

Figure 3. The Fmu MTase Domain and Motif Interactions with AdoMet

(A) A ribbon diagram of the MTase domain colored from blue to red corresponding from N-terminal to C-terminal end. The AdoMet cofactor, in stick representation with carbon atoms colored gray, is positioned at the base of the β sheet. Also shown are the conserved ProCys residues of motif IV (magenta) and the ThrCys of motif VI (cyan).

(B) A cartoon demonstrating the folded topology of the MTase domain, in the same orientation and color scheme as the ribbon diagram above. The motifs containing conserved residues that interact with AdoMet are highlighted. The topology cartoon was generated using TopDraw (C.S. Bond, personal communication).

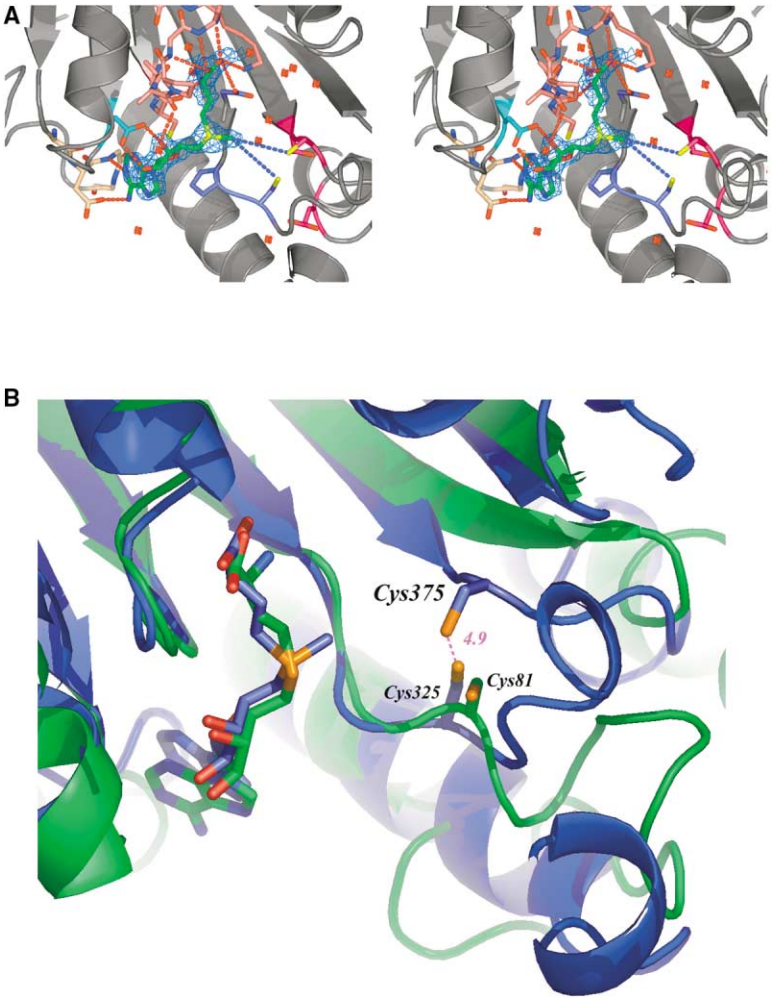

Figure 4. AdoMet Binding and the Conserved Cysteine Residues

(A) A ribbon diagram demonstrating the AdoMet binding site of the MTase domain of Fmu, with AdoMet and the various AdoMet binding motifs shown in ball-and-stick representation. The motifs are represented by differential coloring of the carbon atoms: AdoMet (green), motif I (salmon), motif II (cyan), motif III (wheat), motif IV (slate), and motif VI (magenta). An initial σ_a-weighted ($3|F_o| - 2|F_c|$) difference density map (blue) (i.e., before refinement of AdoMet), calculated at 2.1 Å resolution with FFT (CCP4, 1994) and contoured at 3 σ, is superimposed onto the AdoMet cofactor. The side chains of Cys 325 and Cys 375 are positioned within 6 Å of the activated methyl of the AdoMet cofactor (blue dotted lines).

(B) An overlay of the structure of the Fmu-AdoMet binary complex (blue) with the structure of HhaI DNA m5C MTase (1MHT; green) in complex with DNA and AdoHCys (Klimasauskas et al., 1994) showing the AdoMet binding pocket. The overall position of the AdoMet in Fmu is similar to that of AdoHCys in the HhaI ternary complex structure, suggesting that AdoMet is bound to Fmu in a productive mode. The side chain of the conserved Cys 325 of Fmu is in the same overall position within the active site as the catalytic Cys 81 of HhaI DNA m5C MTase, while the conserved Cys 375, the catalytic residue of Fmu, is slightly closer to the activated methyl of the AdoMet cofactor. The Sγ atoms of Cys 325 and Cys 375 are 4.9 Å apart, as indicated by the dotted line (magenta).

Two Conserved Cysteines in Fmu

The RNA m5C MTase family demonstrates two conserved cysteine residues that lie within the active site of the MTase domain: Cys 325 in the ProCys dipeptide within motif IV and the catalytic Cys 375 in the ThrCys dipeptide within motif VI. In the Fmu structure, Cys 375 is the first residue of a turn that follows β9, with the thiol sulfur within 4.9 Å from the activated methyl group of AdoMet. The side chain of Cys 375 is directed toward the active site cleft in both the apoenzyme and binary complex structures, and the orientation of this residue is stabilized by hydrogen bonding and packing interactions between conserved residues within motif VI. Specifically, the hydroxyl group of Thr 374 makes two specific hydrogen bonds that stabilize the backbone of the polypeptide chain, one with the backbone nitrogen of Ser 376 and the other to the amide oxygen of the side chain of Asn 382.

The other conserved cysteine residue, Cys 325, is located at the end of β8 and, based upon a superimposition with the HhaI DNA m5C MTase, it aligns with the position of the catalytic Cys 81 (Figure 4B). The sulfhydryl of Cys 325 is also positioned at the base of the active site cleft, 5.7 Å away from the activated methyl group of AdoMet and approximately 3.5 Å from the sulfhydryl group of Cys 375. The residues do not appear to form a disulfide bridge in either the apoenzyme or binary complex structures, as attempts to refine a disulfide bond between these atoms resulted in an increase in the R_{free}. Instead, the close proximity of two conserved cysteine nucleophiles to the activated methyl group of the cofactor suggests that both residues could have a role in catalysis.

Based on analogy to the DNA m5C MTases, it was initially proposed that the Cys 325 within the ProCys of motif IV would serve as the catalytic nucleophile in the RNA m5C MTase family (Reid et al., 1999). This notion was compatible with a mutational analysis of Nop2p, a member of subfamily II of the RNA m5C MTases found in *Saccharomyces cerevisiae* (Reid et al., 1999) where site-directed mutants of the cysteine in the ProCys motif resulted in a lethal phenotype, while mutants of the cysteine in the ThrCys motif had only a subtle affect on growth. However, in Fmu, subsequent biochemical analysis of site-directed mutants demonstrated unequivocally that Cys 375 of motif VI is the catalytic nucleophile (Liu and Santi, 2000). In this work, a Cys375Ala mutant enzyme did not methylate C967 of 16S RNA, nor did it form a covalent bond with an RNA substrate substituted with 5-fluoro-cytosine (5-FC), while a Cys325Ala mutant

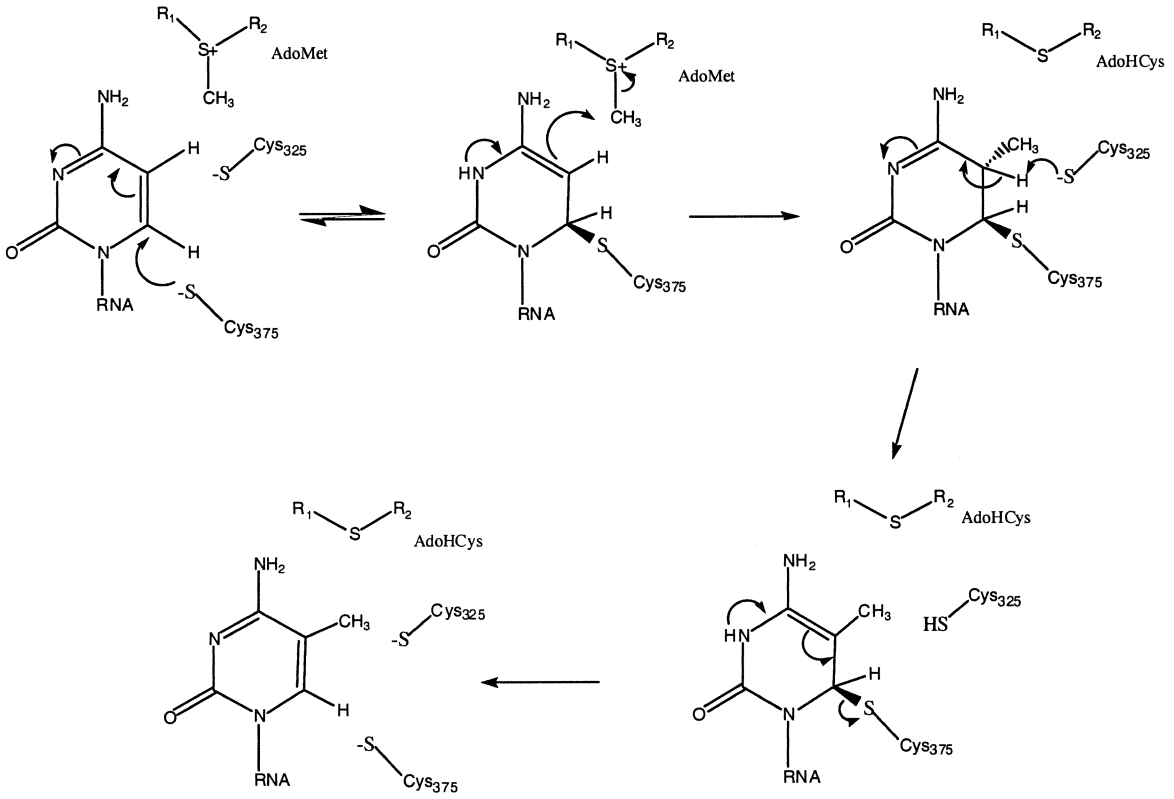

Figure 5. Reaction Scheme for Fmu

Catalysis of m5C formation is driven by nucleophilic attack at the 6-carbon of C967 by the thiolate moiety of Cys 375 of Fmu. Formation of the covalent Michael adduct leads to activated 5-carbon of the nucleoside and results in methyl transfer from the reactive methylthiol of the AdoMet cofactor. This model scheme proposes that Cys 325 acts as the general base in the β elimination step. The stereochemistry is based on structural modeling of the base within the active site.

enzyme retained the ability to methylate the target base and to form a covalent bond with the 5-FC-substituted substrate. Still, the Cys325Ala Fmu does have reduced specific activity (~3-fold), suggesting a secondary role for this residue in catalysis. Recently King and Redman have obtained data that support assignment of the motif VI Cys as the catalytic nucleophile (King and Redman, 2002). Their experiments use mutants of Nop2p and the more easily obtained Ncl1p, another m^{5}C MTase from *S. cerevisiae*. The Ncl1p motif IV mutant enzyme retained detectable methyltransferase activity while the motiv VI mutant enzyme did not. Further, they observed high molecular weight complexes of both proteins on SDS gels when the motif IV cysteine was mutated. With the Ncl1p motif IV mutant, they were able to demonstrate that these were RNA-protein complexes. Motif VI mutants do not form these SDS-stable RNA-protein complexes. They surmise that the stable RNA-protein complexes result in a block in the processing of rRNA, providing a basis for the lethality of the motif IV cysteine mutants. They proposed a model that assigns the general function of aiding RNA release to the motif IV cysteine.

The Fmu structure we have presented here with its unusual arrangement of two nearby cysteine residues within the active site allows us to propose a more specific model for the reaction mechanism of the RNA m^{5}C MTases (Figure 5). Like other enzymes that methylate the C5 of pyrimidines, Fmu activates the C5 of the pyrimidine ring via Michael adduct formation at C6 using Cys 375 as the catalytic nucleophile. The geometry of the active site makes it likely that the subsequent addition of the methyl group of AdoMet occurs in *trans*. Following attachment of the methyl group, a general base is required to abstract the proton at C5 and resolve the covalent complex. In the DNA m^{5}C MTase HhaI, a conserved water molecule is proposed to carry out this function (O'Gara et al., 1996). The finding of stable RNA-protein complexes in the yeast enzymes that are mutated at the residue corresponding to Cys 325 suggests that this residue is involved in product release (King and Redman, 2002). The location and orientation of Cys 325 in the Fmu structure suggest that the motif IV cysteine has the potential to act as the general base in the β elimination of a proton from the methylated cytosine ring. If Cys 325 is fulfilling the proposed role, the positions of Cys 375 and Cys 325 support nucleophilic attack and β elimination occurring on the same side of the pyrimidine ring.

Targeting C967 of 16S rRNA

Although the various RNA m^{5}C MTase enzyme families are likely to target distinct RNA structures, it is expected that they utilize a common sequence motif for cytosine recognition. In the DNA m^{5}C MTases, residues in motifs

VI and VIII function in the recognition and positioning of the target cytosine base. Within motif VI, a conserved carboxylic acid residue (Glu 119) forms hydrogen bonds to the N3 and N4 atoms of the target cytosine base, while Arg165 of motif VIII hydrogen bonds O2 of the cytosine (O'Gara et al., 1996). In the initial assignment of conserved sequence motifs (Reid et al., 1999), it was suggested that a conserved acid at the end of motif VI of the RNA m5C MTases (Glu 381 of Fmu) might perform a similar function. However, this residue is buried within a loop underneath the Fmu active site and is inaccessible to both solvent and presumably to the bound rRNA stem loop.

While it is plausible that there is a conformational change between the N1 and MTase domains upon binding RNA that allows for the repositioning of the motif VI loop to interact with the target base, alternative residues could also function in base recognition. One possibility is that Asp 322, a conserved residue that precedes the ProCys of motif IV and lies at the end strand β8, performs this function. This residue, which forms part of the AdoMet binding pocket and makes a hydrogen bond to the cofactor, superimposes with the sidechain of Glu 119 in the HhaI structure. Another candidate for an acidic residue that could fulfill the role of the HhaI Glu 119 in Fmu is D420 in motif VIII, which corresponds to the conserved Arg 165 of HhaI. Because these two enzymes use different catalytic Cys residues, the cytosine is likely to be positioned differently within the catalytic pocket, possibly with the positions of C5 and C6 switched relative to these positions in HhaI.

Fmu and other members of subfamily I of RNA m5C MTases specifically target C967, a base within a conserved loop following helix 31 of 16S rRNA. Previous biochemical experiments have shown that Fmu cannot methylate unmodified 30S subunits of the ribosome (Weitzmann et al., 1991); however, Fmu can modify position C967 of both in vitro-transcribed 16S rRNA and an in vitro-transcribed 56 nucleotide fragment of 16S (nucleotides 927–982 of 16S rRNA) (Gu et al., 1999). Thus, it is likely that Fmu acts upon 16S rRNA prior to formation of the mature 30S subunit.

To gain structural insight into how Fmu might recognize its specific target RNA, we manually docked and minimized a model for the 56 nucleotide fragment from the known structure of *Thermus thermophilus* 16S rRNA (Schluenzen et al., 2000) into the active site cleft of Fmu (Figures 6A and 6B). The target cytosine base was positioned between both Cys 375 and the activated methyl group of AdoMet. Although the docked model demonstrated both charge and structural complementarity between Fmu and 16S rRNA, it did not take into account conformational flexibility of either Fmu or 16S rRNA, which could both undergo conformational changes possibly resulting in a more stable complex structure.

In order to explore the conformational space of the complex and determine the stability of the model, molecular dynamics were performed. Restrained molecular dynamics were used to refine the docked model structure's local conformation such that it satisfied a set of distance constraints necessary for catalytic activity. Unrestrained molecular dynamics were then run on the refined complex structure to assess the stability and feasibility of the complex structure. The results of the MD simulation (data not shown) indicated that the modeled complex was both structurally feasible and energetically stable. The minimized model demonstrated that the RNA stem loop would easily fit into the cleft, resulting in extensive interactions between the charged phosphate backbone of the RNA with the electropositive surface generated by the N-terminal domain and the N1 domain (Figure 6C). Based on the structure of Fmu and the known structure for this portion of 16S RNA, the model is therefore consistent with a specific mode of binding folded RNA.

Conclusion

The structure of Fmu provides the first look at a member of the RNA m5C MTase family and gives insight into the mechanism of methylation and recognition of the target cytosine base within the specific three-dimensional fold of the 16S rRNA substrate. The structure features a novel arrangement of two conserved cysteine residues positioned near the AdoMet cofactor, with Cys 375 appropriately oriented to serve as the catalytic nucleophile. The position and orientation of the nearby Cys 325 suggests a model for the reaction mechanism in which this residue serves as the base in the β elimination of a proton from the methylated cytosine ring. The structure also reveals two RNA binding domains associated with a methyltransferase core which together generate a positively charged cleft capable of binding the RNA stem loop of 16S RNA containing the target base C967. Based on the shape of the cleft and the position of the active site cysteine and AdoMet cofactor within the cleft, we propose that both putative RNA binding domains interact with the RNA substrate to guide the target cytosine base into the active site.

Experimental Procedures

Protein Production and Crystallization

The cloning of the *fmu* gene and expression of the wild-type protein was carried out as described (Gu et al., 1999). Selenomethionine-labeled Fmu used for MAD phasing experiments was expressed from 4 liters of BL21 (DE3) pLysS cells as per the method of Van Duyne (Van Duyne et al., 1993). To purify the SeMet-labeled Fmu, the cells were pelleted and resuspended in 50 ml buffer A (20 mM Tris HCl [pH 7.5], 50 mM NaCl, 1 mM $MgCl_2$, 5 mM DTT, 10% glycerol) and lysed by sonication. The lysate was cleared by centrifugation for 20 min at 12,000 rpm and the supernatant applied to a preequilibrated 30 ml Q-sepharose column (buffer A). The column was washed with ~10 column volumes of buffer A, and the protein eluted with a gradient of 0–0.5 M KCl in buffer A. After checking the column fractions by SDS-PAGE, the protein was pooled and dialyzed overnight against buffer B (10 mM KPi [pH 6.8], 0.5 mM EDTA, 5 mM DTT, 10% glycerol). The dialyzed sample was applied to a hydroxyapatite column preequilibrated with buffer B and eluted with a linear gradient of 0.01–0.5 M KPi (pH 6.8) in buffer B. The pooled fractions were dialyzed against buffer B, concentrated to ~6 mg/ml, and stored at −80°C.

Crystallographic Data Collection

All Fmu crystals were grown from 2 to 5 mg/ml protein against a reservoir of 14%–16% PEG 4000 and 0.1 M Tris (pH 8.0–8.6) using the hanging-drop vapor diffusion method. For the formation of the Fmu-AdoMet complex, protein was mixed at a 1:1 M ratio with AdoMet at room temperature prior to crystallization. Under the crystallization conditions, native and Fmu-AdoMet crystals grew as rectangular plates with the dimensions $0.05 \times 0.05 \times 0.075$ mm^3, while

A

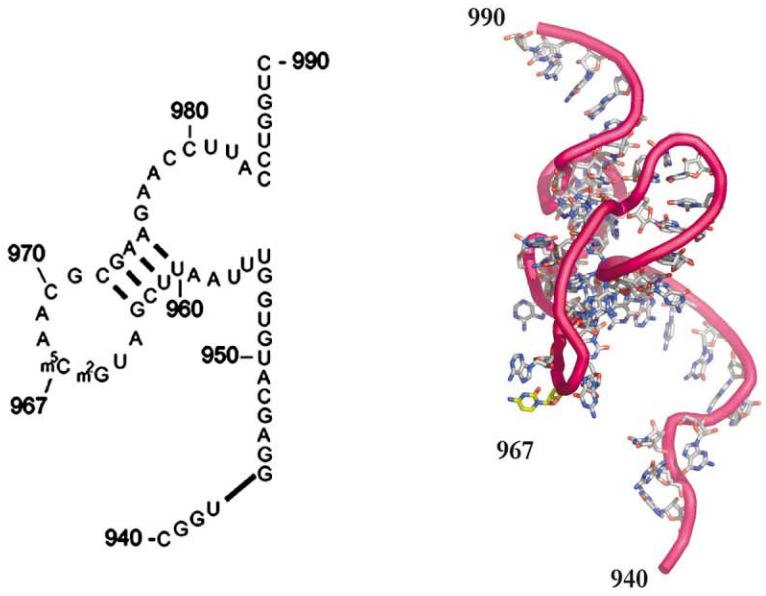

B

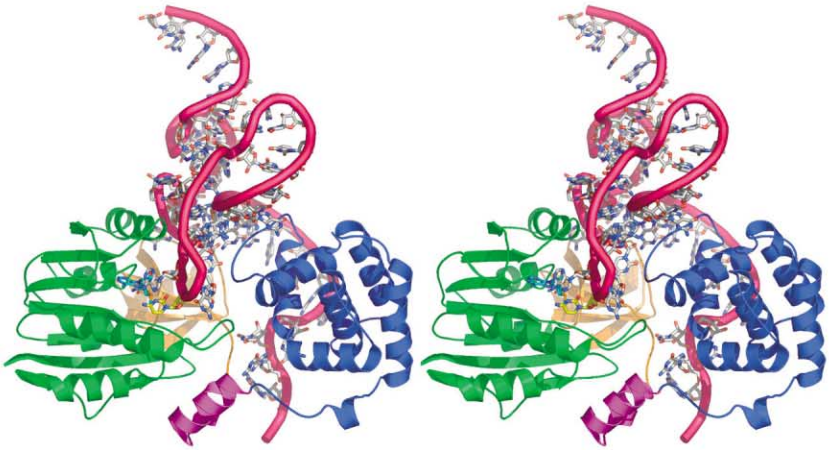

C

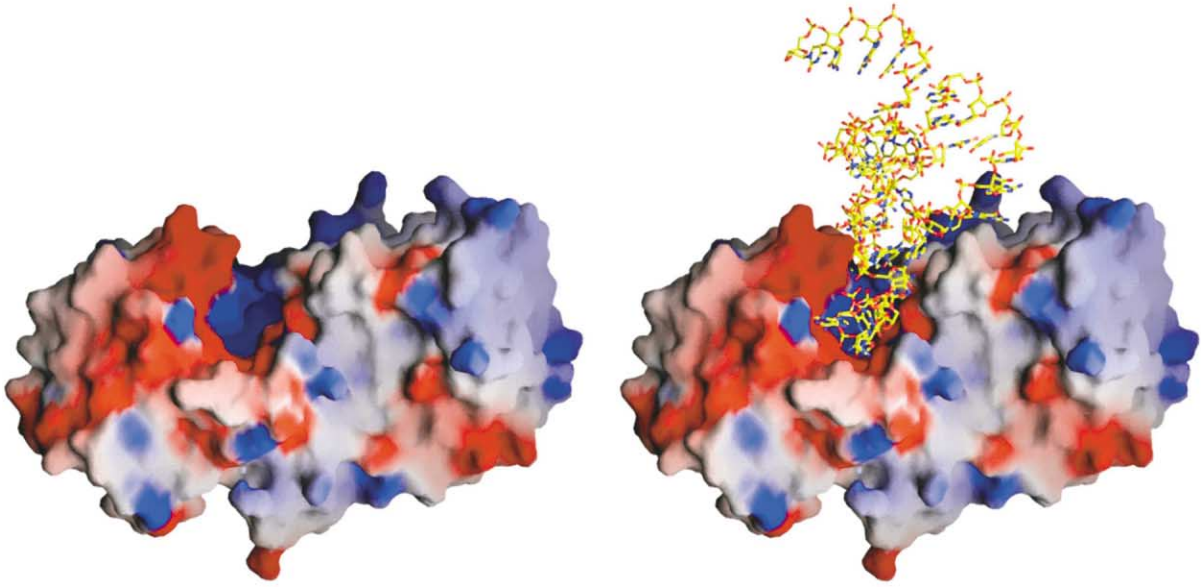

the Se-Met crystals were much larger and grew as incomplete cylindrical rods. Prior to data collection, all Fmu crystals were transferred to mineral oil, then flash cooled to −170°C. Native Fmu and Fmu-AdoMet data were collected to 1.65 and 2.0 Å, respectively, at the Stanford Synchrotron Radiation Laboratory (Beamline 9-1; λ = 0.921) using an ADSC CCD detector and a 1° oscillation per image. Both crystallized in the space group $P2_1$, containing one molecule per asymmetric unit, with unit cell dimensions of a = 59.48 Å, b = 48.64, Å c = 86.65 Å, and β = 108.59° for the native data and a = 57.03 Å, b = 49.00 Å, c = 87.00 Å, and β = 108.45° for the Fmu-AdoMet complex. The three-wavelength MAD data were measured to 2.25 Å from a single SeMet Fmu crystal at the Advanced Light Source (Beamline 5.0.2) with each wavelength collected over two 90° sweeps separated by 180° in φ, using an ADSC CCD detector and a 1° oscillation per image. The Se-Met Fmu protein also crystallized in space group $P2_1$, but with a slight change in packing that resulted in two molecules per asymmetric unit and cell dimensions of a = 87.53 Å, b = 48.56 Å, c = 114.83 Å, and β = 107.79°. All data were reduced with the HKL suite of programs and the individual data sets imported into both the CCP4 and CNS crystallographic program suites.

Structure Determination and Refinement

Anomalous and dispersive difference Patterson maps were calculated for the SeMet Fmu data using CNS, from which a heavy atom positional search gave solutions for eight of the nine selenium atoms. Heavy atom positional refinement and subsequent phase calculations were conducted using the maximum-likelihood phasing program SHARP, and examination of residual difference Fourier maps revealed no additional sites. Phase improvement via iterative density modification and NCS averaging was performed on the data (wavelength 1) using a modified solvent-flattening protocol in the program SOLOMON (Abrahams, 1996) and resulted in 2.25 Å electron density maps with readily interpretable features. Using the graphics program QUANTA (Oldfield, 2002), ~80% of the model was built into the density; subsequently, this model was used for molecular replacement into the 1.65 Å native data in the program AMORE (CCP4, 1994). A density modification procedure was applied in CNS (Brünger et al., 1998), and additional model building was performed in QUANTA (Oldfield, 2002). After the first round of refinement, R_{cryst} = 34.1% and R_{free} = 36.8% (5% of the data). Subsequent refinement cycles were repeated using the standard maximum likelihood target function and simulated annealing-torsion angle dynamic refinement followed by 100 cycles of Powell minimization; with anisotropic temperature factor and bulk solvent correction. Three cycles of this protocol improved the model/data agreement to an R_{cryst} = 23.6% and R_{free} = 27.4% (5% of the data). Using the same R_{free} set of reflections, TLS refinement was carried out in Refmac5 (CCP4, 1994), followed by individual isotropic B factor refinement which gave an R_{cryst} = 21.8% and R_{free} = 25.6%. The density for residues Met 1-Lys 4 and Lys 429 were disordered and were not included in the final model.

Fmu-AdoMet Complex Structure

The structure of the Fmu apoenzyme was used as a search model for molecular replacement for the 2.0 Å Fmu-AdoMet complex data carried out in the program AMORE (CCP4, 1994). The CNS program package was used for rigid body refinement and the resultant R factors were: R_{cryst} = 37.5% and R_{free} = 38.7% (8% of the data), and the resulting difference maps gave unequivocal density for the cofactor. A density modification procedure was applied in CNS, and model building was performed in QUANTA (Oldfield, 2002). After the first round of refinement against all the data to 2.0 Å, R_{cryst} = 34.1% and R_{free} = 36.8%. Subsequent refinement cycles were repeated as described above for the unliganded Fmu structure. Two cycles of this protocol improved the model/data agreement to an R_{cryst} = 25.6% and R_{free} = 30.4. Finally, TLS refinement in Refmac5 followed by individual isotropic B factor refinement further improved the model/data agreement to an R_{cryst} = 23.1% and R_{free} = 27.6%. The final Fmu-AdoMet model contains residues 5–429 and 200 waters.

Modelling of Fmu-RNA Complex

A model of the Fmu/16S rRNA step loop complex was created using the structure of Fmu described in this work and the structure of the 56 nucleotide region of 16S rRNA (PDB code 1FKA). The rRNA structure was manually docked as a rigid body to the Fmu structure such that C967 was positioned proximal to both Cys 375 and the activated methyl group of AdoMet.

Molecular Mechanics Model of Complex

The parm99 (Wang et al., 2000b) force field was used to assign parameters for all atoms and bonds in the system, but parameters for the covalent bond between the SG sulfur of Cys 375 in Fmu and the C6 of cytosine 967 were not available, so we assigned these parameters by analogy. The parameters for the AdoMet cofactor were derived using the program ANTECHAMBER (J. Wang et al., 2001, Pap. Am. Chem. Soc., abstract). In order to refine the complex model to satisfy a proposed catalytic mechanism, a set of three distance restraints were applied to the system. The SG atom of Cys 325 was restrained to 3.15 Å of the H5 atom of C967. The C5 atom of C967 was restrained to 3.15 Å of the CH_3 group on AdoMet. The CG atom of Asp 322 was restrained to 3.15 Å of the N4 atom of C967.

All MD simulations used the AMBER all-atom force field parameters with a 9.0 Å nonbonded cutoff, and a 2 fs time step. A constant pressure periodic boundary was used. The SHAKE algorithm (Ryckaert et al., 1977) was used to constrain the lengths of all bonds to hydrogen atoms. The system temperature was regulated with the Berendsen algorithm (Berendsen et al., 1984) using separate solute/solvent scaling factors of 0.5 ps^{-1} and 0.5 ps^{-1} respectively.

Following minimization, 20 ps of MD was run to heat from 0 K to 298 K. The system was run at 298 K for another 20 ps to equilibrate. The system was then run unrestrained for 480 ps.

Acknowledgments

We thank Sanjay Agarwalla for mechanistic discussions and critical reading of the manuscript. This work was funded by a grant from the National Institutes of Health to R.M.S. (GM51232) and a grant from the Department of Defense Breast Cancer Research program to C.R.N. (BC972599).

Received: May 23, 2003
Revised: July 28, 2003
Accepted: August 15, 2003
Published: December 2, 2003

Figure 6. RNA Substrate and a Model for Binding Fmu

(A) The secondary and tertiary structures of a portion of 16S RNA corresponding to the known minimal substrate for *E. coli* Fmu (nucleotides 940–990). The 16S RNA from *T. thermophilus* (PDB code 1FKA) was used as a surrogate for the *E. coli* RNA, with the target cytosine base (C967) highlighted in yellow.

(B) A model for Fmu binding of its folded RNA substrate. A stereo diagram depicts a snapshot of the molecular dynamics of Fmu in complex with the modeled RNA substrate following energy minimization. The individual Fmu domains are colored as in Figure 1, and the AdoMet cofactor is rendered in stick representation with carbons colored cyan.

(C) A molecular surface representation of Fmu, colored by its local electrostatic potential (blue, +8KT; red −8KT) without and with the folded RNA substrate. The portion of the active site cleft that directly contacts the modeled RNA is predominantly electropositive. The surfaces were generated with GRASP (Nicholls, 1992).

References

Abrahams, J.P., and Leslie, A.G.W. (1996). Methods used in the structure determination pf bovine mitochondrial F-1 Atpase. Acta Crystallogr. D *52*, 30–42.

Berendsen, H.J.C., Postma, J.P.M., van Gunsteren, W.F., DiNola, A., and Haak, J.R. (1984). Molecular dynamics with coupling to an external bath. J. Chem. Phys. *81*, 3684–3690.

Brünger, A.T., Adams, P.D., Clore, G.M., DeLano, W.L., Gros, P., Grosse-Kunstleve, R.W., Jiang, J.S., Kuszewski, J., Nilges, M., Pannu, N.S., et al. (1998). Crystallography & NMR system: a new software suite for macromolecular structure determination. Acta Crystallogr. D Biol. Crystallogr. *54*, 905–921.

Bügl, H., Fauman, E.B., Staker, B.L., Zheng, F., Kushner, S.R., Saper, M.A., Bardwell, J.C., and Jakob, U. (2000). RNA methylation under heat shock control. Mol. Cell *6*, 349–360.

Bussiere, D.E., Muchmore, S.W., Dealwis, C.G., Schluckebier, G., Nienaber, V.L., Edalji, R.P., Walter, K.A., Ladror, U.S., Holzman, T.F., and Abad-Zapatero, C. (1998). Crystal structure of ErmC′, an rRNA methyltransferase which mediates antibiotic resistance in bacteria. Biochemistry *37*, 7103–7112.

Cheng, X.D. (1995). DNA modification by methyltransferases. Curr. Opin. Struct. Biol. *5*, 4–10.

Cheng, X., Kumar, S., Klimasauskas, S., and Roberts, R.J. (1993a). Crystal structure of the *Hha*I DNA methyltransferase. Cold Spring Harb. Symp. Quant. Biol. *58*, 331–338.

Cheng, X., Kumar, S., Posfai, J., Pflugrath, J.W., and Roberts, R.J. (1993b). Crystal structure of the *Hha*I DNA methyltransferase complexed with S-adenosyl-L-methionine. Cell *74*, 299–307.

CCP4 (Collaborative Computation Project 4) (1994). The CCP4 suite: programs for protein crystallography. Acta Crystallogr D *50*, 760–763.

Fauman, E.B., Blumenthal, R.M., and Cheng, X. (1999). Structure and evolution of AdoMet-dependent methyltransferases. In S-Adenosylmethionine-Dependent Methyltransferases: Structures and Functions, X. Cheng and R.M. Blumenthal, eds. (River Edge NJ: World Scientific), pp. 1–54.

Gopal, B., Haire, L.F., Cox, R.A., Jo Colston, M., Major, S., Brannigan, J.A., Smerdon, S.J., and Dodson, G. (2000). The crystal structure of NusB from *Mycobacterium tuberculosis*. Nat. Struct. Biol. *7*, 475–478.

Gu, X.R., Gustafsson, C., Ku, J., Yu, M., and Santi, D.V. (1999). Identification of the 16S rRNA m^5C967 methyltransferase from *Escherichia coli*. Biochemistry *38*, 4053–4057.

Gustafson, W.C., Taylor, C.W., Valdez, B.C., Henning, D., Phippard, A., Ren, Y., Busch, H., and Durban, E. (1998). Nucleolar protein p120 contains an arginine-rich domain that binds to ribosomal RNA. Biochem. J. *331*, 387–393.

Holm, L., and Sander, C. (1993). Protein structure comparison by alignment of distance matrices. J. Mol. Biol. *233*, 123–138.

Hong, B., Brockenbrough, J.S., Wu, P., and Aris, J.P. (1997). Nop2p is required for pre-rRNA processing and 60S ribosome subunit synthesis in yeast. Mol. Cell. Biol. *17*, 378–388.

Ivanetich, K.M., and Santi, D.V. (1992). 5,6-dihydropyrimidine adducts in the reactions and interactions of pyrimidines with proteins. Prog. Nucleic Acid Res. Mol. Biol. *42*, 127–156.

Kealey, J.T., and Santi, D.V. (1991). Identification of the catalytic nucleophile of tRNA (m^5U54)methyltransferase. Biochemistry *30*, 9724–9728.

King, M.Y., and Redman, K.L. (2002). RNA methyltransferases utilize two cysteine residues in the formation of 5-methylcytosine. Biochemistry *41*, 11218–11225.

Kleywegt, G.J., and Jones, T.A. (1997). Detecting folding motifs and similarities in protein structures. Methods Enzymol. *277*, 525–545.

Klimasauskas, S., Kumar, S., Roberts, R.J., and Cheng, X. (1994). *Hha*I methyltransferase flips its target base out of the DNA helix. Cell *76*, 357–369.

Liu, Y., and Santi, D.V. (2000). m^5C RNA and m^5C DNA methyl transferases use different cysteine residues as catalysts. Proc. Natl. Acad. Sci. USA *97*, 8263–8265.

Nicholls, A. (1992). GRASP Manual (New York: Columbia University).

O'Gara, M., Klimasauskas, S., Roberts, R.J., and Cheng, X. (1996). Enzymatic C5-cytosine methylation of DNA: mechanistic implications of new crystal structures for HhaI methyltransferase-DNA-doHcy complexes. J. Mol. Biol. *261*, 634–645.

Oldfield, T. (2002). Pattern-recognition methods to identify secondary structure within X-ray crystallographic electron-density maps. Acta Crystallogr D *58*, 487–493.

Perlaky, L., Busch, R.K., and Busch, H. (1996). Combinatorial effects of monoclonal anti-p120 antibody (MAbp120), liposomes and hyperthermia on MCF-7 and LOX tumor cell lines. Oncol. Res. *8*, 363–369.

Reid, R., Greene, P.J., and Santi, D.V. (1999). Exposition of a family of RNA m^5C methyltransferases from searching genomic and proteomic sequences. Nucleic Acids Res. *27*, 3138–3145.

Rozenski, J., Crain, P.F., and McCloskey, J.A. (1999). The RNA modification database: 1999 update. Nucleic Acids Res. *27*, 196–197.

Ryckaert, J.P., Ciccotti, G., and Berendsen, H.J.C. (1977). Numerical integration of the Cartesian equations of motion for a system with constraints: molecular dynamics of n-alkanes. J. Comput. Phys. *23*, 327–341.

Sato, K., Nishi, T., Takeshima, H., Kochi, M., Kuratsu, J., Masuko, N., Sugimoto, Y., Yamada, Y., and Ushio, Y. (1999). Expression of p120 nucleolar proliferating antigen in human gliomas and growth suppression of glioma cells by p120 ribozyme vector. Int. J. Oncol. *14*, 417–424.

Schluckebier, G., Kozak, M., Bleimling, N., Weinhold, E., and Saenger, W. (1997). Differential binding of S-adenosylmethionine S-adenosylhomocysteine and Sinefungin to the adenine-specific DNA methyltransferase M.*Taq*I. J. Mol. Biol. *265*, 56–67.

Schluenzen, F., Tocilj, A., Zarivach, R., Harms, J., Gluehmann, M., Janell, D., Bashan, A., Bartels, H., Agmon, I., Franceschi, F., et al. (2000). Structure of functionally activated small ribosomal subunit at 3.3 Å resolution. Cell *102*, 615–623.

Tscherne, J.S., Nurse, K., Popienick, P., Michel, H., Sochacki, M., and Ofengand, J. (1999). Purification, cloning, and characterization of the 16S RNA m^5C967 methyltransferase from *Escherichia coli*. Biochemistry *38*, 1884–1892.

Van Duyne, G.D., Standaert, R.F., Karplus, P.A., Schreiber, S.L., and Clardy, J. (1993). Atomic structures of the human immunophilin FKBP-12 complexes with FK506 and rapamycin. J. Mol. Biol. *229*, 105–124.

Wang, H., Boisvert, D., Kim, K.K., Kim, R., and Kim, S.H. (2000a). Crystal structure of a fibrillarin homologue from *Methanococcus jannaschii*, a hyperthermophile, at 1.6 Å resolution. EMBO J. *19*, 317–323.

Wang, J., Cieplak, P., and Kollman, P.A. (2000b). How well does a restrained electrostatic potential (RESP) model perform in calcluating conformational energies of organic and biological molecules. J. Comput. Chem. *21*, 1049–1074.

Weitzmann, C., Tumminia, S.J., Boublik, M., and Ofengand, J. (1991). A paradigm for local conformational control of function in the ribosome: binding of ribosomal protein S19 to *Escherichia coli* 16S rRNA in the presence of S7 is required for methylation of m^2G966 and blocks methylation of m^5C967 by their respective methyltransferases. Nucleic Acids Res. *19*, 7089–7095.

Yusupov, M.M., Yusupova, G.Z., Baucom, A., Lieberman, K., Earnest, T.N., Cate, J.H., and Noller, H.F. (2001). Crystal structure of the ribosome at 5.5 Å resolution. Science *292*, 883–896.